RSC Advances

COMMUNICATION

View Article Online
View Journal | View Issue

Cite this: *RSC Adv.*, 2015, **5**, 80353

Received 2nd September 2015
Accepted 11th September 2015

DOI: 10.1039/c5ra17813d

www.rsc.org/advances

Embedding SiO_2 into graphene oxide *in situ* to generate 3D hierarchical porous graphene laminates for high performance lithium–sulfur batteries†

Wangliang Wu,[ab] Chunying Wan,[ab] Chuxin Wu[ab] and Lunhui Guan*[ab]

3D hierarchical porous graphene laminates (GLs) with high surface area and porosity were synthesized through self-assembly of functionalized graphene oxide embedded with SiO_2 *in situ*. Thus, as a cathode material for Li–S batteries, the obtained GLs loaded with 73 wt% sulfur, deliver a high discharge capacity of 800 mA h g^{-1} after 100 cycles at a current density of 0.2C.

High energy density rechargeable batteries are receiving significant attention to address emerging energy needs in electric vehicles and large-scale renewable energy storage.[1,2] Lithium–sulfur batteries (Li–S), as one of the most promising candidates, have been under intense scrutiny in virtue of their high theoretical capacity (1675 mA h g^{-1}), high natural abundance, low cost and environmental friendliness.

However, the Li–S cell is greatly plagued with problems that have hindered its widespread practical application: (i) low sulfur utilization due to the insulating nature of sulfur and its discharge products, (ii) fast capacity fade and short cycle life due to severe polysulfide diffusion into electrolyte and then shuttle between cathode and anode and (iii) damage of the mechanical integrity and the stability for the electrodes due to the huge volume change of active material during discharge/charge processes.[3–5] To overcome the several persistent drawbacks, sulfur is always combined with a carbon matrix[6–8] or conductive polymer[9,10] to enhance the electrical conductance of the electrodes and thereby improve the performance of the batteries.

Graphene, as one of the most fascinating carbon material owing to its unique two dimensional morphology, high specific surface area, superior electrical conductivity, and excellent mechanical property, is often used to reinforce the overall conductivity of the electrode for Li–S batteries.[11] Recently, some studies have been investigated to synthesize the graphene–sulfur composite.[12] In addition, sandwich-like graphene–sulfur nanocomposites are also designed to enhance the performance of Li–S batteries.[13,14] However, the huge surface area and strong π–π interactions between graphene layers lead to their facile stacking.[15] Hence, these sulfur–graphene hybrids show poor cycling stability. To further improve the specific capacities and stabilities of the sulfur–graphene electrodes. Some researchers propose strategies that the sulfur nanoparticles are coated with the graphene or GO to confine the sulfur and suppress the dissolution of polysulfides into electrolyte.[16,17] Nevertheless, the sulfur enveloped by the graphene or GO is still partially insulating and results in the electrode with low rate capability. Ding *et al.* report a method to synthesize a porous graphene for immobilizing the sulfur by chemically tailoring the graphene with KOH.[18] Zhao *et al.* show an intrinsically unstacked double-layer template graphene with mesoporous *via* template-directed chemical vapour deposition, as a promising carbon material for Li–S batteries.[15] As a consequence, the high capacity and excellent cycling retention can be realized. Thus, design a rational graphene-based porous carbon to combine the excellent properties of graphene with porous architectures is an efficient approach to improve the performance of Li–S batteries.[19–21]

Herein, we report novel 3D hierarchical porous graphene laminates (GLs) with high pore volume and large surface area as a carbon host material for sulfur cathode. The GLs composite with layer structure, not only possesses excellent external accessible surface area and high pore volume to confine the polysulfides in the cathodes during the discharge/charge processes, but also affords a 3D conductive network for ion/electron transportation. Whereupon, the GLs–S composite with 73 wt% sulfur content exhibits high reversible capacity, stable cycling performance as well as excellent rate capabilities and cycling efficiency. At a current density of 0.2C, it demonstrates a high discharge capacity of 800 mA h g^{-1} after 100 cycles. Even at a high rate of 1C, it still remains a reversible capacity of 596 mA h g^{-1} after 200 cycles.

[a]*Key Laboratory of Design and Assembly of Functional Nanostructures, Chinese Academy of Sciences, Fuzhou, Fujian 350002, China. E-mail: guanlh@fjirsm.ac.cn; Fax: +86-591-63173550; Tel: +86-591-63173550*

[b]*Fujian Key Laboratory of Nanomaterials, Fuzhou, Fujian 350002, China*

† Electronic supplementary information (ESI) available. See DOI: 10.1039/c5ra17813d

The synthetic strategy of GLs is illustrated in Fig. 1. The GLs composite was synthesized through self-assembly of functionalized GO embedded with SiO_2 *in situ* as a pore forming agent. Firstly, GO-SiO_2 nanosheets were fabricated by functionalized GO self-assembled with GO as the shape-directing agent and SiO_2 nanoparticles (NPs) as the mesopore guides. Scanning electron microscopy (SEM) reveals that the GO-SiO_2 possesses a model sandwich-like structure in Fig. 2a and d. The SiO_2 NPs are homogeneously immobilized onto the surface of GO. In addition, transmission electron microscopy (TEM) shows that the size of SiO_2 NPs synthesized *in situ* onto the GO is ~10 nm in Fig. 3a and d. Then, GLs were created by a carbonization process followed by HF solution etching. As described in Fig. 2b and e, the GLs are constructed by GO nanosheets stacking. Moreover, the thin layer pore walls can be identified from TEM in Fig. 3b and e, revealing that the porous nanocages are comprised of rGO nanosheets. Finally, GLs–S composite was synthesized by a simple melt infiltration method. After sulfur infiltration, the resultant composite inherits the 3D porous graphene laminates morphology with no obvious structural change in Fig. 2c and f and 3c and f. The distributing status of S is further investigated by the homogenous EDS mapping of GLs–S composite in Fig. S1.†

Nitrogen adsorption–desorption isotherms are used to investigate the porous structures of the GLs, GLs–S, rGO and rGO–S composites in Fig. 4a. The GLs exhibits combined characteristics of type II/IV, with a Brunauer–Emmett–Teller (BET) surface area of 771 $m^2\ g^{-1}$ and a total pore volume of 1.53 $cm^3\ g^{-1}$, which are higher than the values of 252 $m^2\ g^{-1}$ and 1.12 $cm^3\ g^{-1}$ for rGO. The GLs composite possessing higher surface area and pore volume could facilitate to retain polysulfides from dissolving into the electrolyte and thus improve the cycle stability due to a strong physical adsorption of the porous structure for the active material and soluble polysulphides. After sulfur impregnation, the hysteresis region of the GLs–S (or rGO–S) almost disappears, corresponding to a systematic decrease of the BET surface area and the total pore volume of GLs–S (or rGO–S) composite, as summarized in Table 1 (ESI).† The tremendous changes in the surface area and porosity of the samples reconfirm that S is indeed dispersed in the pores of GLs (or rGO), which is consistent with the pore size distribution curves in Fig. 4b. Moreover, the GLs present more abundant mesopores than these of rGO, well matched with the TEM observation result in Fig. 3b and e.

The overall content of sulfur in GLs–S sample was measured to be as high as 73 wt% by thermogravimetric analysis (TGA) in Fig. 5a. For comparison, the sulfur loading of rGO–S was just 68 wt%. The detailed structures are also checked by the XRD patterns of the GLs, GLs–S, rGO and rGO–S composites in Fig. 5b. The GLs and rGO exhibit a diffraction peak near 26°and 42°, corresponding to the (002) and (100) peaks of graphene.[22] It is consistent with the detecting graphene sheet pore walls in Fig. 3e. Meanwhile some crystalline sulfur peaks with orthorhombic structure (JCPDS 08-0247) can be observed from GLs–S and rGO–S composites, indicating the distribution of ultrafine sulfur in the composites.

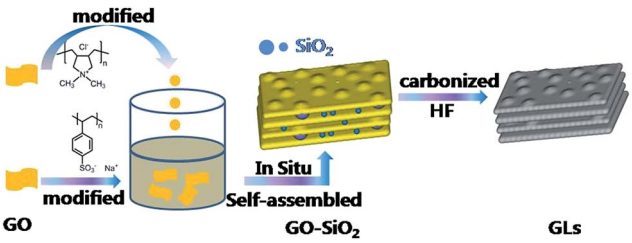

Fig. 1 Schematic illustration of the synthesis procedure of GLs composite.

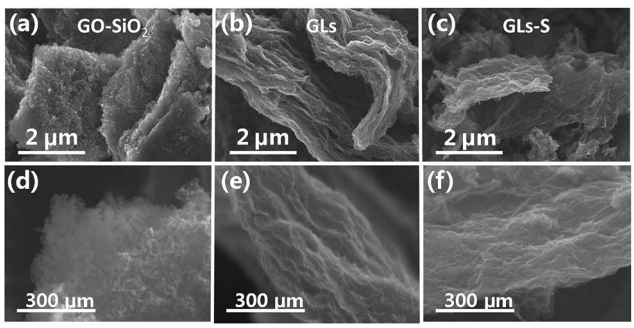

Fig. 2 SEM images of (a and d) GO-SiO_2, (b and e) GLs and (c and f) GLs–S.

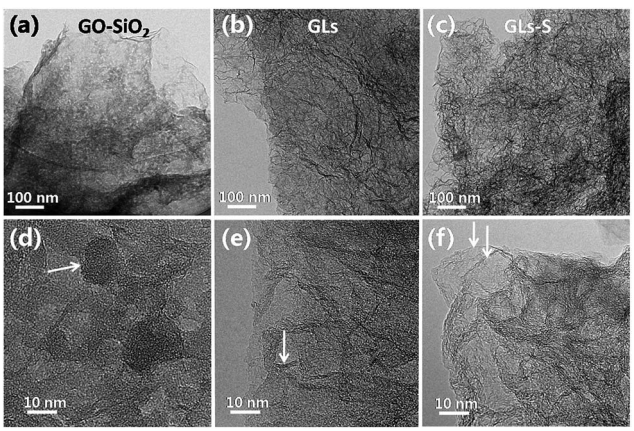

Fig. 3 TEM images of (a and d) GO-SiO_2, (b and e) GLs and (c and f) GLs–S.

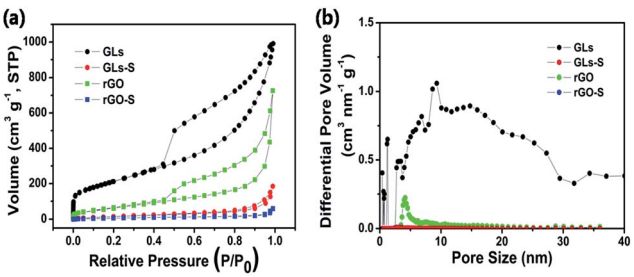

Fig. 4 (a) Nitrogen adsorption–desorption isotherms and (b) pore size distribution of GLs, GLs–S, rGO and rGO–S composites.

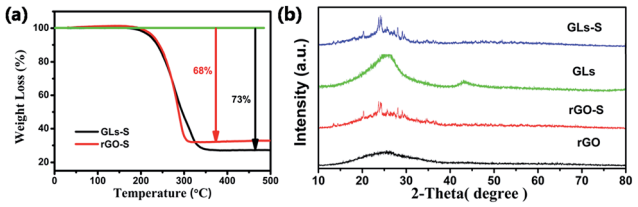

Fig. 5 (a) TGA curves of GLs–S and rGO–S composites and (b) XRD patterns of GLs, GLs–S, rGO and rGO–S composites.

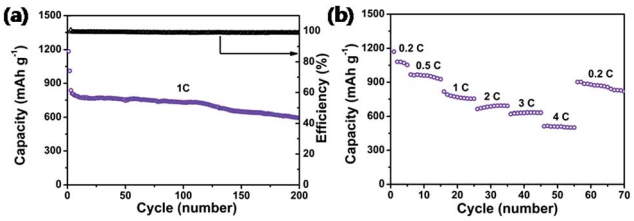

Fig. 7 (a) Cycle performance at a high current density of 1C and (b) rate capability of the GLs–S composite.

The lithiation voltage curves of the GLs–S composite are exhibited in Fig. 6a at 0.2C (1C = 1675 mA g^{-1}) between 1.9 V and 2.7 V. The curves demonstrate two main plateaus of typical sulfur cathode at 2.3 V and 2.1 V, which are attributed to the transformation of sulfur into long-chain polysulphides (Li_2S_n; where n is typically 4–8) and further conversion of short-chain polysulphides (Li_2S_2/Li_2S), respectively.[10] The two step lithiation process is in correspondence well with redox peaks displayed in the CV curves in Fig. S2.† Fig. 6b shows the cycling stabilities of the GLs–S composite. The GLs–S electrode exhibits the initial discharge capacity of 1158 mA h g^{-1} and retains a reversible capacity of 800 mA h g^{-1} at 0.2C rate after 100 cycles, which is higher than the values for sulfur combined with porous carbons,[23–25] hollow carbon spheres,[26,27] carbon nanofibers/nanotubes,[28,29] graphene/GO,[30,31] as well as graphene-based hybrid.[32–34] In contrast, the rGO–S electrode suffers from rapid capacity fading during the cycles and only remains a discharge capacity of 629 mA h g^{-1} after 100 cycles, implying severe polysulfides dissolution. The significantly higher capacity and coulombic efficiency of GLs–S electrode compared with rGO–S reaffirm that the GLs with large electrochemically active surface area and high pore volume, provides the intimate contact with S to suppress the dissolution of the polysulphides and also affords a 3D conductive network for ion/electron transportation.

In addition, the cycling performance at a high current density of 1C is also examined in Fig. 7a. After being discharged/charged at 0.2C for the first two cycles, the cell shows a very good capacity retention, which maintains a reversible capacity of 596 mA h g^{-1} after 200 cycles. These results indicate that the design of such porous layer structure could indeed improve the performance of Li–S batteries. The rate capability of the GLs–S composite from 0.2 to 4C is carried out in Fig. 7b. The discharge capacity of composite is stabilized around 1050 mA h g^{-1} at 0.2C. Even at a high rate of 4C, the composite also delivers a high capacity of 510 mA h g^{-1}. When the rate is switched abruptly back from 4 to 0.2C, the discharge capacity can be mostly recovered at 818 mA h g^{-1} after 70 cycles, indicating the good stability of the GLs–S structure. The excellent electrochemical performance can be understood through the following reasons: Firstly, the GLs structure consisting of two dimensional graphene offered superior 3D electrical conductive network to facilitate fast electronic/ionic transport and enhance reaction kinetics of sulfur, resulting good rate capabilities. Secondly, the GLs composite with mesopore nanocages and high surface area can effectively prevent lithium polysulfides from dissolving into electrolyte, resulting in stable cycling retention and high efficiency. Thirdly, the large pore volume of GLs can accommodate more sulfur to improve the energy density of batteries. Finally, the wrinkles in the GLs composite possess high stretch ability could buffer the strain generated from the volumetric changes of sulfur during the discharge/charge processes and therefore keep the structure stable.

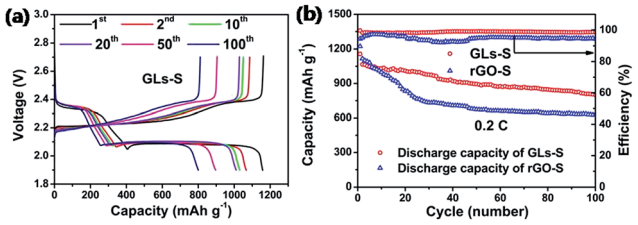

Fig. 6 (a) Typical voltage capacity profiles of GLs–S and (b) cycle stability of GLs–S and rGO–S at 0.2C.

Conclusions

In summary, we have successfully synthesized 3D hierarchical porous GLs through self-assembly of functionalized GO embedded with SiO_2 *in situ* as a pore forming agent. Due to the unique architecture of GLs with large pore volume and high surface area, the obtained GLs–S cathode exhibits outstanding electrochemical performance. It shows excellent cycling stability and retains a reversible capacity of 800 mA h g^{-1} at 0.2C after 100 cycles and 596 mA h g^{-1} at 1C after 200 cycles. Even at a high rate of 4C, it still delivers a capacity of 510 mA h g^{-1}. The synthesis strategy is simple and facile, conceptually providing new opportunities for materials to design 3D porous architectures that can be extended to many different electrode materials.

Acknowledgements

We acknowledge the financial support provided by the National Key Project on Basic Research (Grant no. 2011CB935904), the National Natural Science Foundation of China (Grant no. 21171163, 91127020), Science and Technology Planning Project of Fujian Province (Grant No. 2014H2008) and NSF for Distinguished Young Scholars of Fujian Province (Grant no. 2013J06006).

Notes and references

1 P. G. Bruce, S. A. Freunberger, L. J. Hardwick and J. M. Tarascon, *Nat. Mater.*, 2012, **11**, 19–29.
2 G. Zhou, L. Li, C. Ma, S. Wang, Y. Shi, N. Koratkar, W. Ren, F. Li and H.-M. Cheng, *Nano Energy*, 2015, **11**, 356–365.
3 X. Ji and L. F. Nazar, *J. Mater. Chem.*, 2010, **20**, 9821.
4 S. H. Chung and A. Manthiram, *Adv. Mater.*, 2014, **26**, 7352–7357.
5 Z. Wei Seh, W. Li, J. J. Cha, G. Zheng, Y. Yang, M. T. McDowell, P. C. Hsu and Y. Cui, *Nat. Commun.*, 2013, **4**, 1331.
6 X. Ji, K. T. Lee and L. F. Nazar, *Nat. Mater.*, 2009, **8**, 500–506.
7 H. Chen, C. Wang, W. Dong, W. Lu, Z. Du and L. Chen, *Nano Lett.*, 2015, **15**, 798–802.
8 W. Zhou, C. Wang, Q. Zhang, H. D. Abruña, Y. He, J. Wang, S. X. Mao and X. Xiao, *Adv. Energy Mater.*, 2015, 1401752.
9 F. B. Dias, L. Plomp and J. B. J. Veldhuis, *J. Power Sources*, 2002, **88**, 169–191.
10 W. Zhou, Y. Yu, H. Chen, F. J. DiSalvo and H. D. Abruna, *J. Am. Chem. Soc.*, 2013, **135**, 16736–16743.
11 H. Kim, H.-D. Lim, J. Kim and K. Kang, *J. Mater. Chem. A*, 2014, **2**, 33–47.
12 J.-Z. Wang, L. Lu, M. Choucair, J. A. Stride, X. Xu and H.-K. Liu, *J. Power Sources*, 2011, **196**, 7030–7034.
13 Y. Cao, X. Li, I. A. Aksay, J. Lemmon, Z. Nie, Z. Yang and J. Liu, *Phys. Chem. Chem. Phys.*, 2011, **13**, 7660–7665.
14 B. Wang, K. Li, D. Su, H. Ahn and G. Wang, *Chem.–Asian J.*, 2012, **7**, 1637–1643.
15 M. Q. Zhao, Q. Zhang, J. Q. Huang, G. L. Tian, J. Q. Nie, H. J. Peng and F. Wei, *Nat. Commun.*, 2014, **5**, 3410.
16 J. Rong, M. Ge, X. Fang and C. Zhou, *Nano Lett.*, 2014, **14**, 473–479.
17 S. Evers and L. F. Nazar, *Chem. Commun.*, 2012, **48**, 1233–1235.
18 B. Ding, C. Yuan, L. Shen, G. Xu, P. Nie, Q. Lai and X. Zhang, *J. Mater. Chem. A*, 2013, **1**, 1096–1101.
19 X. Yang, L. Zhang, F. Zhang, Y. Huang and Y. Chen, *ACS Nano*, 2014, **8**, 5208–5215.
20 X. A. Chen, Z. Xiao, X. Ning, Z. Liu, Z. Yang, C. Zou, S. Wang, X. Chen, Y. Chen and S. Huang, *Adv. Energy Mater.*, 2014, **4**, 1301988.
21 Z. Peng, W. Fang, H. Zhao, J. Fang, H. Cheng, T. N. L. Doan, J. Xu and P. Chen, *J. Power Sources*, 2015, **282**, 70–78.
22 M. S. Park, J. S. Yu, K. J. Kim, G. Jeong, J. H. Kim, Y. N. Jo, U. Hwang, S. Kang, T. Woo and Y. J. Kim, *Phys. Chem. Chem. Phys.*, 2012, **14**, 6796–6804.
23 B. Zhang, X. Qin, G. R. Li and X. P. Gao, *Energy Environ. Sci.*, 2010, **3**, 1531.
24 X. Li, Y. Cao, W. Qi, L. V. Saraf, J. Xiao, Z. Nie, J. Mietek, J.-G. Zhang, B. Schwenzer and J. Liu, *J. Mater. Chem.*, 2011, **21**, 16603.
25 H. Sohn, M. L. Gordin, T. Xu, S. Chen, D. Lv, J. Song, A. Manivannan and D. Wang, *ACS Appl. Mater. Interfaces*, 2014, **6**, 7596–7606.
26 C. Zhang, H. Bin Wu, C. Yuan, Z. Guo and X. W. D. Lou, *Angew. Chem., Int. Ed.*, 2012, 9592–9595.
27 Y. Qu, Z. Zhang, X. Wang, Y. Lai, Y. Liu and J. Li, *J. Mater. Chem. A*, 2013, **1**, 14306.
28 G. Zhou, D.-W. Wang, F. Li, P.-X. Hou, L. Yin, C. Liu, G. Q. Lu, I. R. Gentle and H.-M. Cheng, *Energy Environ. Sci.*, 2012, **5**, 8901.
29 J.-Q. Huang, Q. Zhang, S.-M. Zhang, X.-F. Liu, W. Zhu, W.-Z. Qian and F. Wei, *Carbon*, 2013, **58**, 99–106.
30 H. Wang, Y. Yang, Y. Liang, J. T. Robinson, Y. Li, A. Jackson, Y. Cui and H. Dai, *Nano Lett.*, 2011, **11**, 2644–2647.
31 C. Xu, Y. Wu, X. Zhao, X. Wang, G. Du, J. Zhang and J. Tu, *J. Power Sources*, 2015, **275**, 22–25.
32 S. Lu, Y. Cheng, X. Wu and J. Liu, *Nano Lett.*, 2013, **13**, 2485–2489.
33 M.-Q. Zhao, X.-F. Liu, Q. Zhang, G.-L. Tian, J.-Q. Huang, W. Zhu and F. Wei, *ACS Nano*, 2012, **6**, 10759–10769.
34 X. Huang, B. Sun, K. Li, S. Chen and G. Wang, *J. Mater. Chem. A*, 2013, **1**, 13484.

